



Numerical simulation of finite strain viscoplastic problems[☆]

C. García Garino^{a,*}, M.S. Ribero Vairo^a, S. Andía Fagés^b, A.E. Mirasso^{a,b}, J.-P. Ponthot^c

^a Facultad de Ingeniería and ITIC, Universidad Nacional de Cuyo, Centro Universitario, M5502JMA, Mendoza, Argentina

^b Facultad Regional Mendoza, Universidad Tecnológica Nacional, Rodríguez 273, 5500 Mendoza, Argentina

^c Aerospace and Mechanical Engineering Department, University of Liege, B4000, Liege, Belgium

ARTICLE INFO

Article history:

Received 3 February 2012

Received in revised form 2 September 2012

Keywords:

Viscoplasticity

Perzyna's model

Hyperelastic approach

Large strain

Finite elements

ABSTRACT

A large strain elastoplastic constitutive model based on hyperelasticity and multiplicative decomposition of deformation gradient tensor is extended to viscous case, in a framework similar to the one that has been proposed by Ponthot in an hypoelastic context. In this way a very useful framework can be obtained, able to deal with both rate dependent and rate independent problems.

In this work a review of theoretical details and numerical implementation of the model are discussed. Similarly to what is done in rate independent plasticity, a Newton–Raphson scheme has been used to solve the non linear consistency condition in order to compute the viscoplastic multiplier.

A plane strain plate with a central circular hole under tension is simulated in order to test the proposed model. Large deformation effects are considered in all the simulations carried out. Different parameters of the constitutive model are varied in order to study the sensitivity of the proposed algorithm.

© 2012 Elsevier B.V. All rights reserved.

1. Introduction

This paper presents results of a large strain viscoplastic model based on hyperelasticity. The large strain model structure is taken from previous work of García Garino and Oliver [1,2], derived in the context of the ideas of Simo and Ortiz [3] and Simo [4,5] for the rate independent case. The viscoplastic extension comes from a work of Ponthot [6], based on Perzyna type model [7], where a unified algorithm for elasto/viscoplastic problems has been proposed. However the work of Ponthot relies on a hypoelastic formulation while here a hyperelastic model is chosen.

A complete review of the state of the art is not included in this work due to limited space, but a comprehensive account of the viscoplastic problem can be found in the textbooks of Lubliner [8], for the fundamentals, and Ottosen and Ristinmaa [9] and Simo and Hughes [10] both for theory and numerical discussion. For small strain problems Carosio and coauthors [11] have discussed the problem for, according authors classification, continuum and consistent viscoplasticity and Alfano et al. [12] presented general solution procedures in elasto/viscoplasticity. In some works rate dependent Perzyna models are discussed in the framework of large strain models: besides the cited work of Ponthot [6], Wang and Sluys [13] have proposed an incremental model for the elastic problem and the integration of the problem is carried out using a midpoint rule. Simo and Hughes [10] have discussed the problem for a Duvaut–Lyons model type.

[☆] This work has been partially supported by Argentinean ANPCyT, project PAE-PICT-2007-2312, and National University of Cuyo, projects 06/B194 and Seismic Vulnerability of Structures Research Program.

* Corresponding author. Tel.: +54 2614291000; fax: +54 2614494086.

E-mail addresses: cgarino04@gmail.com, cgarcia@itu.uncu.edu.ar (C. García Garino), aemirasso@uncu.edu.ar (A.E. Mirasso), JP.Ponthot@ulg.ac.be (J.-P. Ponthot).

The kinematics of the resultant constitutive model is based on the multiplicative decomposition of the deformation gradient tensor [14]. Stresses are derived from a hyperelastic potential and the model is written in the framework of internal variables theory and thermodynamics of irreversible solids [8]. The stress update algorithm proposed by Ponthot [6] treats the elasto/viscoplastic problem in a unified way. For a J2-flow material model, it is a simple generalization to rate-dependent problems of the classical radial return algorithm [10] for rate-independent plasticity, including a generalized consistency condition.

The classical *elastic predictor–plastic corrector* split problem [5,10] is used in order to derive a numerical time integration scheme of the model. In this way a fully implicit algorithm is designed. The resultant update algorithm is written in terms of kinematics quantities instead of the stress tensor, as it is usually presented in the literature. In this work it is shown that the unified elasto/viscoplastic stress update proposed by Ponthot [6] is naturally included in the (pre-existent) numerical structure of the rate independent case.

The integration scheme proposed in this work is both inexpensive and accurate. In addition, it allows us to write down a closed-form expression for the so-called consistent (visco) elastoplastic tangent modulus. Use of this consistent modulus (and not the continuum one) for the establishment of the global tangent stiffness matrix is essential in preserving the quadratic rate of convergence in Newton's procedure required by implicit algorithms [15].

Therefore, it exhibits all its (good) properties, including accuracy, stability and existence of a consistent tangent operator. Moreover the algorithm is unified in the sense that the same routines are able to integrate both elasto-plastic and elasto-viscoplastic models. The former case is simply obtained by setting the viscosity parameter to zero.

In this work a problem proposed in the literature, see Alfano et al. [12] for instance, is simulated for a large strain case. Different values of viscoplastic constitutive parameters are chosen in order to study the proposed model behavior.

2. Large strain elastoplastic model

At this point the proposed constitutive model is briefly presented. The elastoplastic constitutive model [1,2] can be written in three different configurations. However for the purpose of this work it is enough to present the results in the current configuration. First, the main kinematics results are introduced followed by a summary of constitutive equations. Finally the particular case of an elastoplastic model for metals is discussed.

2.1. Kinematics

The kinematics of the problem is based on the very well known multiplicative decomposition of deformation gradient tensor \mathbf{F} into its elastic \mathbf{F}^e and plastic \mathbf{F}^p components [14], as it is shown in Eq. (1).

$$\mathbf{F} = \mathbf{F}^e \mathbf{F}^p. \quad (1)$$

The Almansi strain tensor \mathbf{e} and its elastic and plastic components, \mathbf{e}^e and \mathbf{e}^p , respectively, are the variables used in the constitutive model. The total Almansi strain and its elastic component are defined in Eq. (2).

$$\mathbf{e} = \frac{1}{2}(\mathbf{g} - \mathbf{b}^{-1}) \quad \mathbf{e}^e = \frac{1}{2}(\mathbf{g} - \mathbf{b}^{e-1}) \quad (2)$$

where the spatial metric tensor is denoted as \mathbf{g} , the Finger tensor is defined as $\mathbf{b}^{-1} = \mathbf{F}^{-T} \mathbf{F}^{-1}$ and its elastic component as $\mathbf{b}^{e-1} = \mathbf{F}^{e-T} \mathbf{F}^{e-1}$.

The rate of deformation tensor \mathbf{d} is obtained by computing the Lie derivative L_v [16] of Almansi strain tensor, and it admits an additive decomposition into its elastic and plastic components $\mathbf{d} = \mathbf{d}^e + \mathbf{d}^p$.

2.2. Constitutive model

In this section the equations that define the constitutive model in the current configuration are presented.

$$\mathbf{e} = \mathbf{e}^e + \mathbf{e}^p \quad (3)$$

$$\mathbf{d} = \mathbf{d}^e + \mathbf{d}^p \quad (4)$$

$$\boldsymbol{\sigma} = \frac{\partial \psi^e(\mathbf{e}^e, \mathbf{b}^{e-1})}{\partial \mathbf{e}^e} \quad (5)$$

$$\mathbf{d}^p = \dot{\gamma} \frac{\partial g}{\partial \boldsymbol{\sigma}} \quad (6)$$

$$\mathcal{D}^p = \boldsymbol{\tau} : \mathbf{d}^p + \mathbf{p} : \dot{\boldsymbol{\alpha}} \geq 0 \quad (7)$$

$$\dot{\gamma} \geq 0 \quad f \leq 0 \quad \dot{\gamma} f = 0 \quad (8)$$

where $\boldsymbol{\sigma}$ denotes the Cauchy stress tensor, $\psi^e(\mathbf{e}^e, \mathbf{b}^{e-1})$ is the elastic free energy, f and g account for yield criteria and plastic potential, respectively, and $\dot{\gamma}$ is the plastic multiplier. Plastic dissipation is denoted by \mathcal{D}^p and $\boldsymbol{\alpha}$ and \mathbf{p} are a proper set of internal variables and their conjugate thermodynamical forces, respectively.

2.3. Constitutive model for metals

Elastic strains always remain small for metals even when submitted to large strains. In this case the tensor \mathbf{F}^e is always close to the Identity. Consequently tensor \mathbf{b}^{e-1} tends to the spatial metric tensor \mathbf{g} . In this case the distinction between intermediate and current configurations has no meaning. Then it is possible to write the elastic component of the free energy function as a quadratic function of elastic component of Almansi strain tensor \mathbf{e}^e and Lamé parameter λ and μ as it is shown in Eq. (9).

$$\psi^e = \left[\frac{1}{2} \lambda \text{tr}(\mathbf{e}^e)^2 + \mu (\mathbf{e}^e : \mathbf{e}^e) \right]. \quad (9)$$

From Eq. (5) the Cauchy stress tensor results in:

$$\boldsymbol{\sigma} = \lambda \text{tr}(\mathbf{e}^e) \mathbf{1} + 2 \mu \mathbf{e}^e. \quad (10)$$

This model has been used previously by the authors [1,2] as an alternative to the neohookean models proposed by Simo and Ortiz [3] and Simo [4,5]. Plasticity is taken into account by means of an associative flow rule for which $f = g$. The yield function is the very well known Von Mises or J2 model given by Eq. (11).

$$f(\boldsymbol{\sigma}, \sigma_y) = \bar{\sigma} - \sigma_y = 0 \quad (11)$$

where $\bar{\sigma} = \sqrt{\frac{3}{2} \mathbf{s} : \mathbf{s}}$ \mathbf{s} denotes equivalent stress, \mathbf{s} is the deviatoric Cauchy stress tensor and σ_y is the current yield stress. Flow rule can now be written in terms of the yield criteria f as:

$$\mathbf{d}^p = \dot{\gamma} \mathbf{n} \quad \text{where } \mathbf{n}_{ij} = \frac{\mathbf{s}_{ij}}{\sqrt{\mathbf{s}_{kl} \mathbf{s}_{kl}}} \quad (12)$$

where \mathbf{n} denotes the unit outward normal ($\mathbf{n} : \mathbf{n} = 1$) to the yield surface and the plastic multiplier $\dot{\gamma}$ can be computed from the Kuhn Tucker conditions given in Eq. (8).

The hardening law relates yield stress evolution $\dot{\sigma}_y$ to the rate of the effective plastic strain $\dot{\bar{\epsilon}}^p$, defined as $\dot{\bar{\epsilon}}^p = \sqrt{\frac{2}{3}} \mathbf{d}^p : \mathbf{d}^p$, as it is shown in Eq. (13).

$$\dot{\sigma}_y = h \dot{\bar{\epsilon}}^p = \sqrt{\frac{2}{3}} h \dot{\gamma} \quad (13)$$

where h denotes the material parameter that corresponds to the slope of the effective stress vs. effective plastic strain curve under uniaxial loading conditions, also known as hardening modulus in the case of a linear hardening for which h is constant.

3. Large strain viscoplastic model

In this section the viscoplastic problem is discussed and theoretical results derived in previous works [6,1] are presented here with emphasis on the flow rule and extended consistency condition. Main results of the elastoplastic kinematics presented above are still valid taking into account that inelastic variables in this case describe the rate dependent case.

$$\mathbf{e} = \mathbf{e}^e + \mathbf{e}^{vp} \quad \mathbf{d} = \mathbf{d}^e + \mathbf{d}^{vp} \quad (14)$$

where \mathbf{e}^{vp} and \mathbf{d}^{vp} are viscoplastic counterparts of the plastic components of Almansi strain tensor \mathbf{e}^p and rate of deformation tensor \mathbf{d}^p respectively.

Given the uncoupled format chosen for the free energy function its elastic component remains unchanged in this case. Then Cauchy stress is still computed from Eqs. (5) and (9).

Contrary to the case of rate independent plasticity, the effective stress $\bar{\sigma}$ is no longer constrained to remain less or equal to the current yield stress then, it is possible to have here $\bar{\sigma} \geq \sigma_y$. Therefore the *overstress* d is defined as

$$d = \langle \bar{\sigma} - \sigma_y \rangle \quad (15)$$

where $\langle x \rangle$ denotes the Mac Auley brackets. Clearly, an inelastic process can only take place if the overstress d is positive, consequently $f \geq 0$.

For example, classical viscoplastic models of the Perzyna type [7] may be considered as a penalty regularization of the rate-independent plasticity case where the consistency parameter $\dot{\gamma}$ has been replaced by an increasing function of the overstress [6] e.g.

$$\dot{\gamma}^{vp} = \sqrt{\frac{3}{2}} \left\langle \frac{\bar{\sigma} - \sigma_y}{\eta(\bar{\epsilon}^{vp})^{1/n}} \right\rangle^m \quad (16)$$

where $\dot{\gamma}^{vp}$ accounts for the *viscoplastic multiplier*, n is a hardening exponent, m is a rate sensitivity parameter, $\bar{\epsilon}^{vp}$ is the equivalent viscoplastic strain and η is a viscosity parameter.

The effective viscoplastic strain is defined as $\dot{\bar{\epsilon}}^{vp} = \sqrt{\frac{2}{3} \dot{\mathbf{d}}^{vp} : \dot{\mathbf{d}}^{vp}}$. In this case, the evolution equations are still of the form:

$$\dot{\mathbf{d}}^{vp} = \dot{\gamma}^{vp} \mathbf{n} \quad \dot{\bar{\epsilon}}^{vp} = \sqrt{\frac{2}{3}} \dot{\gamma}^{vp} \quad \text{or} \quad \dot{\sigma}_y = h \dot{\bar{\epsilon}}^{vp} \quad (17)$$

which are quite similar to the rate-independent case given in Eqs. (12) and (13). Combining Eqs. (16), and (17) gives:

$$\dot{\bar{\epsilon}}^{vp} = \sqrt{\frac{2}{3}} \dot{\gamma}^{vp} = \left\langle \frac{\bar{\sigma} - \sigma_y}{\eta (\bar{\epsilon}^{vp})^{1/n}} \right\rangle^m \quad (18)$$

so that, in the viscoplastic range, a new constraint is defined [6] as:

$$\bar{f} = \bar{\sigma} - \sigma_y - \eta (\bar{\epsilon}^{vp})^{1/n} (\dot{\bar{\epsilon}}^{vp})^{1/m} = 0. \quad (19)$$

This criterion is a *generalization of the classical Von Mises criterion* $f = 0$ for rate-dependent materials. The rate independent case can simply be recovered by imposing $\eta = 0$ (no viscosity effect), a result that has been already pointed out in the literature by other authors [6,12,9,13]. In the elastic regime, both f and \bar{f} are equivalent since, in that case can be written:

$$\dot{\bar{\epsilon}}^{vp} = 0 \quad \text{and} \quad \bar{\sigma} \leq \sigma_y \quad (20)$$

so that it follows, similarly to plasticity that:

$$\bar{f} \leq 0. \quad (21)$$

Moreover, from relation (16), it can be noted, that as viscosity η goes to zero (rate-independent case), the consistency parameter $\dot{\gamma}^{vp}$ remains finite and positive (though indeterminate) since $\bar{\sigma} - \sigma_y$ also goes to zero. The extended criterion (19) will play a crucial role in the integration algorithm described hereafter. It also allows a generalization of the Kuhn–Tucker conditions which, in the visco-plastic case, can be extended to the following form:

$$\dot{\gamma}^{vp} \bar{f} = 0, \quad \dot{\gamma}^{vp} \geq 0, \quad \bar{f} \leq 0. \quad (22)$$

4. Numerical scheme

In this section the numerical scheme necessary to implement the discussed theoretical model in a finite element code is derived. A synthesis of elastic predictor/plastic corrector (return mapping algorithm) methodology, can be found in Simo [5] and the numerical scheme derived for the large strain elastoplastic model is discussed in [2]. Here this methodology is extended to the time-dependent case following [6] in order to design an *elastic predictor, elasto/viscoplastic corrector* approach. For a given configuration ${}^t\Omega$ defined by its known set of positions ${}^t\mathbf{x}$, where all the state variables are known at time t , the problem is to update all state variables to a new configuration defined by its set of position ${}^{t+\Delta t}\mathbf{x}$ (which are supposed to be known) at time $t + \Delta t$. This situation typically arises in a non linear finite element problem where the new positions ${}^{t+\Delta t}\mathbf{x}$ are determined from a discretized version of the momentum balance equations. These incremental displacements are, in turn, used to calculate the incremental strain history by means of the kinematic relations discussed in Section 2.1.

The problem discussed here is, for the given incremental strain history, to find the new values of the state variables $({}^{t+\Delta t}\sigma, {}^{t+\Delta t}\bar{\epsilon}^{vp}, {}^{t+\Delta t}\sigma_y)$ at ${}^{t+\Delta t}$. These are obtained by integration of the local constitutive equations with initial conditions given by $({}^t\sigma, {}^t\bar{\epsilon}^{vp}, {}^t\sigma_y)$ at t .

In a first step, the elastic predictor problem is solved with initial conditions that are the converged values of the previous time step while keeping irreversible variables frozen. This produce a trial elastic stress state ${}^t\sigma^{TR}$ or ${}^t\sigma^e$ which, if outside the yield surface f is taken as the initial conditions for the solution of the viscoplastic corrector problem. The objective of this second step is to restore consistency by returning back the trial stress to the generalized criterion \bar{f} (and not on the yield function f as it is done in the rate-independent case!).

4.1. Elastic problem

In this problem the viscoplastic quantities remain frozen: $({}^{t+\Delta t}\mathbf{F}^{vpTR} = {}^t\mathbf{F}^{vp})$. The trial (*elastic*) component of the deformation gradient tensor results:

$${}^{t+\Delta t}\mathbf{F}^{eTR} = {}^{t+\Delta t}\mathbf{F} ({}^{t+\Delta t}\mathbf{F}^{vpTR})^{-1} = \mathbf{f} {}^t\mathbf{F} ({}^t\mathbf{F}^{vp})^{-1} = \mathbf{f} {}^t\mathbf{F}^e \quad (23)$$

where $\mathbf{f} = \frac{\partial^{t+\Delta t} \mathbf{x}}{\partial^t \mathbf{x}}$ is the incremental deformation gradient tensor between two successive configurations ${}^t\Omega$ and ${}^{t+\Delta t}\Omega$. The predictor value of the elastic Finger tensor ${}^{t+\Delta t} \mathbf{b}^{e-1TR}$ is thus given by:

$${}^{t+\Delta t} \mathbf{b}^{e-1TR} = \left({}^{t+\Delta t} \mathbf{F}^{e-T} {}^{t+\Delta t} \mathbf{F}^{e-1} \right)^{TR} = \mathbf{f}^{-T} {}^t \mathbf{b}^{e-1} \mathbf{f}^{-1}. \quad (24)$$

The predictor value of the elastic Almansi strain ${}^{t+\Delta t} \mathbf{e}^{eTR} = \frac{1}{2}({}^{t+\Delta t} \mathbf{g} - {}^{t+\Delta t} \mathbf{b}^{e-1TR})$ is computed from the Eq. (24) and the trial stresses $\boldsymbol{\sigma}^{TR}$ are obtained from Eq. (10). Then the value of trial yield function ${}^{t+\Delta t} f^{TR} = {}^{t+\Delta t} \bar{\sigma}^{TR} - {}^t \sigma_y$ must be checked. If ${}^{t+\Delta t} f^{TR} \leq 0$ then the time step is completely elastic and the trial state is the solution of the problem. If, on the other hand, ${}^{t+\Delta t} f^{TR} > 0$, at least a part of the time step is viscoplastic and consistency needs to be restored.

4.2. Viscoplastic problem

In this phase problem the current configuration remains fixed and the internal variables are updated in order to satisfy the constitutive law. For the rate independent problem Simo [5] has proposed to integrate the flow rule in the original configuration. In a similar way can be written here for the rate dependent problem:

$$\dot{\mathbf{C}}^{vp} = 2\phi^* \mathbf{d}^{vp} = 2\dot{\lambda}^{vp} \phi^* \mathbf{n} = 2\dot{\lambda}^{vp} \mathbf{N} \quad (25)$$

where \mathbf{C}^{vp} is the viscoplastic component of right Cauchy Green tensor, $\dot{\lambda}^{vp}$ accounts for the numerical counterpart of viscoplastic multiplier γ^{vp} , \mathbf{N} is the normal vector to the yield function in the original configuration and ϕ^* denotes the pull-back operator [16]. Writing $\dot{\mathbf{C}}^{vp} = \frac{{}^{t+\Delta t} \mathbf{C}^{vp} - {}^t \mathbf{C}^{vp}}{\Delta t}$ and integrating Eq. (25) results:

$${}^{t+\Delta t} \mathbf{C}^{vp} - {}^t \mathbf{C}^{vp} = 2\lambda^{vp} {}^{t+\Delta t} \mathbf{N}. \quad (26)$$

Eq. (26) can be pushed forward to the spatial configuration in order to write an equivalent expression in terms of current variables. Taking into account that $\mathbf{b}^{e-1} = \phi_* \mathbf{C}^{vp}$, see details in [2], ϕ_* denotes the push forward operator, the updated Finger tensor can be computed as:

$${}^{t+\Delta t} \mathbf{b}^{e-1} = {}^{t+\Delta t} \mathbf{b}^{e-1TR} + 2\lambda^{vp} {}^{t+\Delta t} \mathbf{n}. \quad (27)$$

The plastic multiplier λ^{vp} , which is the sole remaining unknown, can be computed using the radial return algorithm as it discussed below.

From Eq. (2) the elastic component of Almansi strain tensor results in terms of the viscoplastic update of elastic Finger tensor given in Eq. (27):

$$\begin{aligned} {}^{t+\Delta t} \mathbf{e}^e &= \frac{1}{2} (\mathbf{g} - {}^{t+\Delta t} \mathbf{b}^{e-1}) = \frac{1}{2} (\mathbf{g} - {}^{t+\Delta t} \mathbf{b}^{e-1TR} - 2\lambda^{vp} {}^{t+\Delta t} \mathbf{n}) \\ &= {}^{t+\Delta t} \mathbf{e}^{eTR} - \lambda^{vp} {}^{t+\Delta t} \mathbf{n}. \end{aligned} \quad (28)$$

Taking into account Eq. (10), the viscoplastic correction of the elastics component of Almansi strain tensor given in Eq. (28) is written in terms of the Cauchy stress tensor as:

$${}^{t+\Delta t} \boldsymbol{\sigma} = {}^{t+\Delta t} \boldsymbol{\sigma}^{TR} - 2\lambda^{vp} \mu {}^{t+\Delta t} \mathbf{n} \quad (29)$$

that is the result shown in Eq. (51), Section 6.3 in the work of Ponthot [6], after integration over the time interval $[t, t + \Delta t]$, with initial conditions given by ${}^t \boldsymbol{\sigma}$, ${}^t \bar{\epsilon}^{vp}$ and ${}^t \sigma_y$.

In order to compute the viscoplastic multiplier λ^{vp} an integration procedure [6] very similar to the radial return method of plasticity is used. The tensor ${}^{t+\Delta t} \mathbf{n}$ is approximated by ${}^{t+\Delta t} \mathbf{n} = \frac{{}^{t+\Delta t} \mathbf{s}^{TR}}{\sqrt{{}^{t+\Delta t} \mathbf{s}^{TR} : {}^{t+\Delta t} \mathbf{s}^{TR}}}$ and the time derivative $\dot{\bar{\epsilon}}^{vp}$ is approached by $\dot{\bar{\epsilon}}^{vp} = \frac{{}^{t+\Delta t} \bar{\epsilon}^{vp} - {}^t \bar{\epsilon}^{vp}}{\Delta t}$, so that the final values are given by

$${}^{t+\Delta t} \bar{\epsilon}^{vp} = {}^t \bar{\epsilon}^{vp} + \dot{\bar{\epsilon}}^{vp} \Delta t = {}^t \bar{\epsilon}^{vp} + \sqrt{\frac{2}{3}} \lambda^{vp} \quad (30)$$

where the (unknown) scalar parameter λ^{vp} stands for

$$\lambda^{vp} = \frac{3}{2} \int_t^{t+\Delta t} \dot{\bar{\epsilon}}^{vp} dt = \int_t^{t+\Delta t} \dot{\lambda} dt. \quad (31)$$

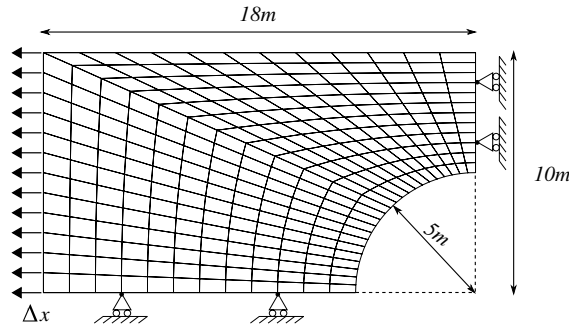


Fig. 1. Plane strain plate with a hole—spatial discretization scheme and boundary conditions.

The λ^{vp} parameter is simply determined by the enforcement of the *generalized discrete consistency condition*, $\bar{f} = 0$, at time $t = t + \Delta t$, i.e.

$$\begin{aligned} \bar{f}(\lambda^{vp}) = & \sqrt{\frac{3}{2} [\mathbf{s}^{TR} - 2\mu \lambda^{vp} \mathbf{n}] : [\mathbf{s}^{TR} - 2\mu \lambda^{vp} \mathbf{n}]} - {}^{t+\Delta t}\sigma_y(\lambda^{vp}) \\ & - \eta \left(\bar{\epsilon}_0^{vp} + \sqrt{\frac{2}{3}} \lambda^{vp} \right)^{\frac{1}{n}} \left(\sqrt{\frac{2}{3}} \frac{\lambda^{vp}}{\Delta t} \right)^{\frac{1}{m}} = 0 \end{aligned} \quad (32)$$

where ${}^{t+\Delta t}\sigma_y$ is a given function of $\bar{\epsilon}^{vp}$ and consequently a given function of λ^{vp} .

The scalar equation (32) is a non linear expression where the only unknown parameter is λ^{vp} . It can be easily solved by a local Newton–Raphson iteration. In the particular case where $n = \infty$ (no multiplicative hardening), $m = 1$ (linear dependence between overstress and viscoplastic rate of deformation), and $h = \text{constant}$ (linear hardening) a closed form solution of this equation is given by $\lambda^{vp} = \frac{1}{2\mu} \frac{\sqrt{\mathbf{s}^{TR}:\mathbf{s}^{TR}} - \sqrt{\frac{2}{3}} {}^t\sigma_y}{1 + \frac{1}{3\mu} (h + \frac{\eta}{\Delta t})}$.

So that it is now obvious that the present algorithm is a generalization to the rate-dependent case of the classical radial return algorithm. This one is exactly recovered (with no numerical difficulty) by setting $\eta = 0$ (no viscosity effect). In the viscous case, one can see that the rate-dependent solution for a *linear* case is equivalent to rate-independent solution with a fictitious hardening given by $h^* = h + \eta/\Delta t$. On the other case when $\eta \rightarrow \infty$ the overstress becomes unbounded and the response of the model tends to the elastic case.

5. Numerical examples

In this section the results of different numerical problems simulated with the proposed model including large strains are discussed. As an application example a plane strain plate with a central circular hole, see Fig. 1, has been chosen because it is a problem previously discussed in the literature, see Alfano et al. [12] and references therein for instance. The geometry consists of a rectangular plate of $20\text{ m} \times 36\text{ m}$ with a 5 m radius hole in its center. Because of the symmetry of the problem it is possible to analyze only one quarter of the sample. The material properties are: $E = 2.1\text{e5 MPa}$, $\nu = 0.3$, $\sigma_{y0} = 240\text{ MPa}$ and $h = 0$. The viscoplastic parameters are changed on each case and $\Delta t = 1\text{ s}$ in all studies. For the spatial discretization a mesh containing 288 Q1P0 mixed elements was used. This element is based on a bilinear approximation, Q1, for the displacements field u plus a constant pressure $P0$ throughout the element. The constant pressure is obtained by computing the pressure at each Gauss point, and then averaging the different results. This element has been successfully used by the authors in many applications [2,6,17].

The imposed displacements are applied in 400 steps of 0.05 m each one, reaching a total of 2.00 m , thus reaching the large strains domain.

Different combinations of constitutive parameters m and η have been selected in order to test the proposed model over a wide range of material behavior. The hardening multiplicative effect has been neglected in all cases by imposing $n \rightarrow \infty$. The viscosity parameter values considered are $\eta = 1\text{e3}, 1\text{e4}, 3\text{e4}, 5\text{e4}, 7\text{e4}, 1\text{e5}, 1\text{e6}, 1\text{e9 MPa s}$ and the chosen sensitivity parameter values are $m = 1, 2, 3, 5$. The two limiting cases such as purely elastic or elastoplastic problems have been considered as well.

For the material data selected, the extended yield function introduced in Eq. (19) leads to:

$$\bar{f} = \bar{\sigma} - \sigma_{y0} - \eta (\dot{\bar{\epsilon}}^{vp})^{1/m} = 0.$$

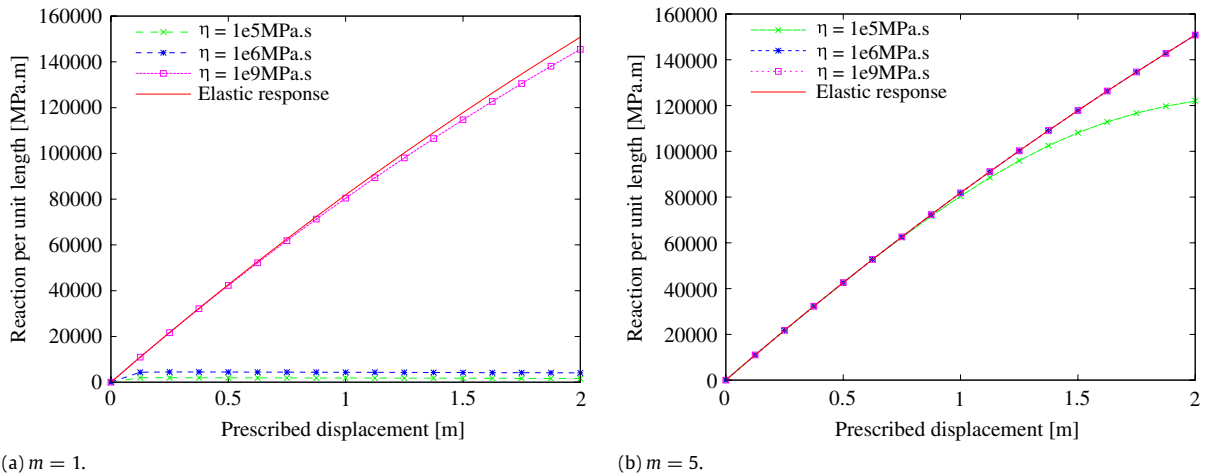


Fig. 2. Elastic limiting cases results for $m = 1, 5$ and $\eta = 1e5, 1e6, 1e9$.

Then the additional viscous resistance $\eta (\dot{\bar{\epsilon}}^{vp})^{1/m}$, that in fact is numerically equal to the overstress d , is proportional to the value of η that is weighted by the factor $(\dot{\bar{\epsilon}}^{vp})^{1/m}$. Considering that $\dot{\bar{\epsilon}}^{vp} = \frac{\Delta \bar{\epsilon}^{vp}}{\Delta t}$ and $\Delta t = 1$ s, provided that $\Delta \bar{\epsilon}^{vp} < 1$ and $m > 1$, the $(\dot{\bar{\epsilon}}^{vp})^{1/m}$ factor increases its value for larger m values and the η effect is magnified.

The obtained results are presented in terms of total reactions P versus imposed displacements u graphs as well as deformed configurations for the different simulations tested. The P vs. u curves are grouped in the so called *elastic* and *elastoplastic limiting* cases because very different values are obtained for P in the simulated problems.

In Fig. 2 Elastic limiting cases results are presented together with the elastic problem response for comparison purposes.

In Fig. 2(a) the response of the model for $m = 1$ and considered η values can be seen. From the curves shown it can be observed that the viscoplastic response for $\eta = 1e9$ tends to the elastic result. The viscoplastic responses are similar for the cases $\eta = 1e5, 1e6$, and the total reaction P reaches very small values in comparison with the case $\eta = 1e9$. It is difficult to obtain more information from this picture due to the different values found for P . However the $\eta = 1e5$ case is included in Fig. 3(a) as well, and it can be clearly seen at the onset of viscoplasticity that there is maximum value for P . Fig. 2(b) displays the graphs for $m = 5$ case, all the simulations included show a response that tend to the elastic problem result. Moreover for $\eta = 1e6, 1e9$ cases the P – u graphs are barely distinguishable from the elastic result. A tendency to reach a maximum value for P can still be observed for $\eta = 1e5$.

In summary, from these results it can be concluded that: (i) The maximum values of the total reaction P increase for larger values of η ; (ii) For a given value of η the maximum values of P increases for larger values of the m parameter.

The result of elastoplastic problem and *elastoplastic limiting* cases for $\eta = 1e3, 1e4, 3e4, 5e4, 7e4, 1e5$ are presented in Fig. 3. The P vs u graphs are shown in Fig. 3(a)–(d) for $m = 1, 2, 3, 5$ respectively.

A marked structural (global) softening behavior is observed for $m = 1$ in Fig. 3(a). The maximum value for the total reaction P reaches 2000 MPa (per unit length) for $\eta = 1e5$ at the onset of viscoplasticity. This effect is similar for all the other considered values of η when $m = 1$. The maximum value of the total reaction P increases for larger values of η in this case as well, and the obtained P value for $\eta = 1e5$, is about 50% larger than the one computed for $\eta = 1e3$. For the case of $m = 2$, shown in Fig. 3(b), two remarks can be stated: (i) For all the cases the total reaction P reaches a maximum value followed by an almost constant curve. A slight structural softening effect can be seen as well; (ii) An important change in the maximum values of P is observed.

The viscoplastic response presented in Fig. 3(c) for $m = 3$ shows a similar behavior to the results previously displayed in Fig. 2(b) for $m = 2$, but the values of P are three times larger in this case. As can be seen in Fig. 3(d) the obtained results for $m = 5$ tend to the elastic response except for the case $\eta = 1e4$.

In Fig. 4 the final deformed shapes for the elastoplastic problem, the viscoplastic model for $m = 1, 5$ and $\eta = 1e4, 1e6$ and the elastic problem, respectively are presented.

In Fig. 4(a) the final deformed shape of the plate for the elastoplastic problem is shown. As can be seen in the picture the area of the central zone has been considerably reduced. The deformation pattern observed in the picture is typical of the necking behavior of tensile bars, see [17] for instance. Moreover, for the three rows of elements closer to the central symmetry line, a remarkable stretching can be observed and its deformation is considerably larger than in any other element in the deformed mesh. The final deformed shape for the viscoplastic model for $m = 1$ and $\eta = 1e4$, displayed in Fig. 4(b), is very similar to the elastoplastic case but the necking is slightly smaller. The deformed shape corresponding to the values $m = 1, \eta = 1e6$ and $m = 5, \eta = 1e4$, shown in Fig. 4(c) and (d) respectively, can be considered as a transition result between the limit problems. In both cases necking is still present but is less pronounced than in deformed shapes presented in Fig. 4(a) and (b). Similar final configurations are found for viscoplastic response for $m = 5, \eta = 1e6$ and elastic problem as

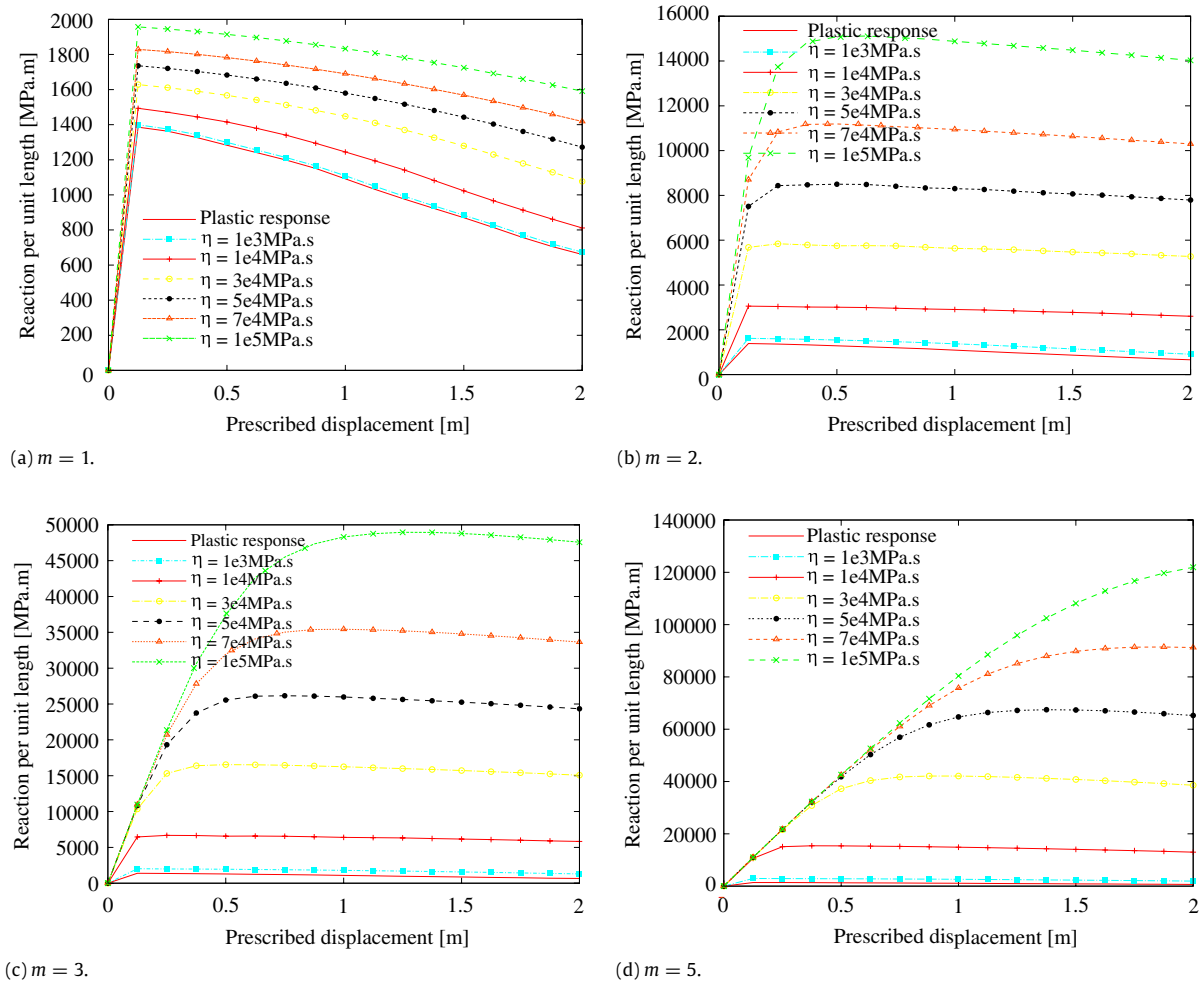


Fig. 3. Elastoplastic limiting cases results for $m = 1, 2, 3, 5$ and $\eta = 1e3, 1e4, 3e4, 5e4, 7e4, 1e5$.

can be seen in Fig. 4(e) and (f), respectively. The stretching of the elements is quite similar in both cases and there is no clear necking effect found. In summary it can be said that deformation and necking effects are larger for lower values of viscosity parameter η . On the other hand, for larger values of the sensitivity parameter m , deformations become smaller and from a qualitative point of view it can be expressed that the viscoplastic response tends to the elastic behavior.

It is important to observe comparatively Figs. 3(a) and 4(b). A global softening behavior can be observed in terms of P vs. u graphs shown in Fig. 3(a) for $m = 1$ and the considered values of viscosity parameter η . Taking into account that there is no viscoplastic material (local) softening for the considered material data, the observed global softening effect can only take place due to a reduction of the current area in the central zone, i.e. necking. In fact this kind of deformation pattern is clearly seen in Fig. 4(b). Notice however, that with respect to the rate independent (elastoplastic) case shown in Fig. 4(a) viscosity acts in the sense of reducing the necking. Besides a reasonably qualitative agreement can be found from Fig. 4(a) and (b) that explains a viscoplastic behavior similar to the elastoplastic response discussed above. This behavior is typical of lower viscosity values like the one considered in the studies shown in the cited figures. From the other pictures presented in Fig. 4 it can be observed that there is no strain concentration like in the previous case, a result which is in agreement with the fact that P vs. u graphs shown in Fig. 3(b)–(d) do not present global softening effects.

6. Mesh sensitivity study

It is well known that non linear material simulations exhibit mesh sensitivity results for certain constitutive models, especially when local material softening appears. Due to geometrical non-linearities, this can also be the case at the structural level, even if the material behavior does not locally exhibit softening. Indeed, in this work an elastic perfectly viscoplastic material ($h = 0$) has been considered and consequently a rather marked necking effect has been found for the inviscid case ($\eta = 0$), as can be seen in Fig. 4(a).

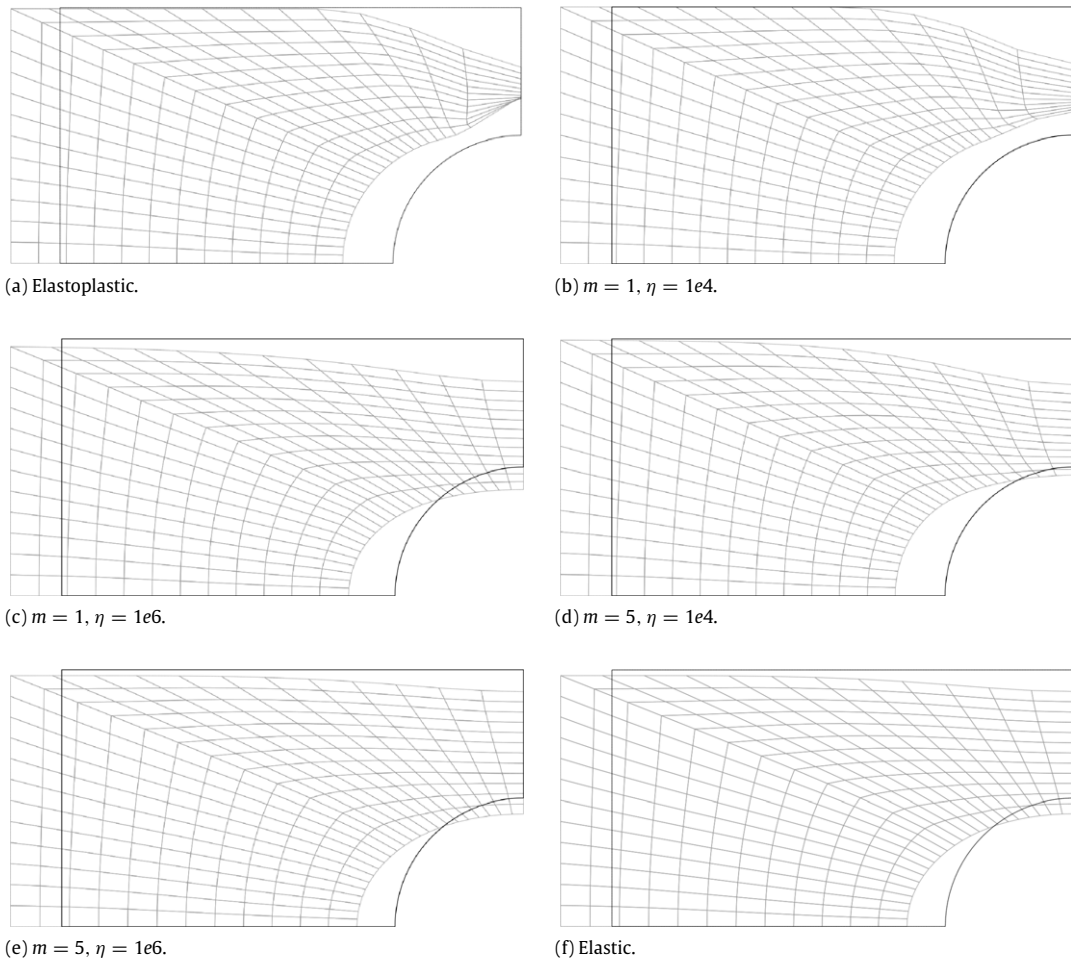


Fig. 4. Final deformed meshes for elastoplastic, viscoplastic and elastic problems.

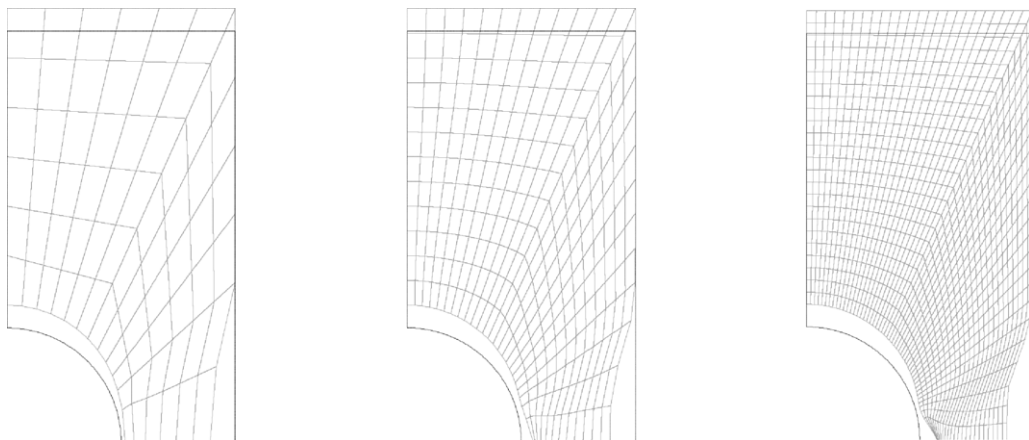


Fig. 5. Final deformed shapes for the different finite element meshes considered (elastoplastic case).

In order to study the sensitivity of the results in terms of the finite element discretization three different meshes have been considered, see Fig. 5. The different meshes considered have been designed in order to conform to a *mesh refinement sequence*, i.e. in the initial configuration, each node of a coarser mesh will be a node of the more refined mesh. The coarser mesh contains only 72 elements built on two different 6×6 elements zones. The intermediate one is the mesh used to obtain the results discussed in the previous section. It has 288 elements based on two 12×12 elements zones. Finally the

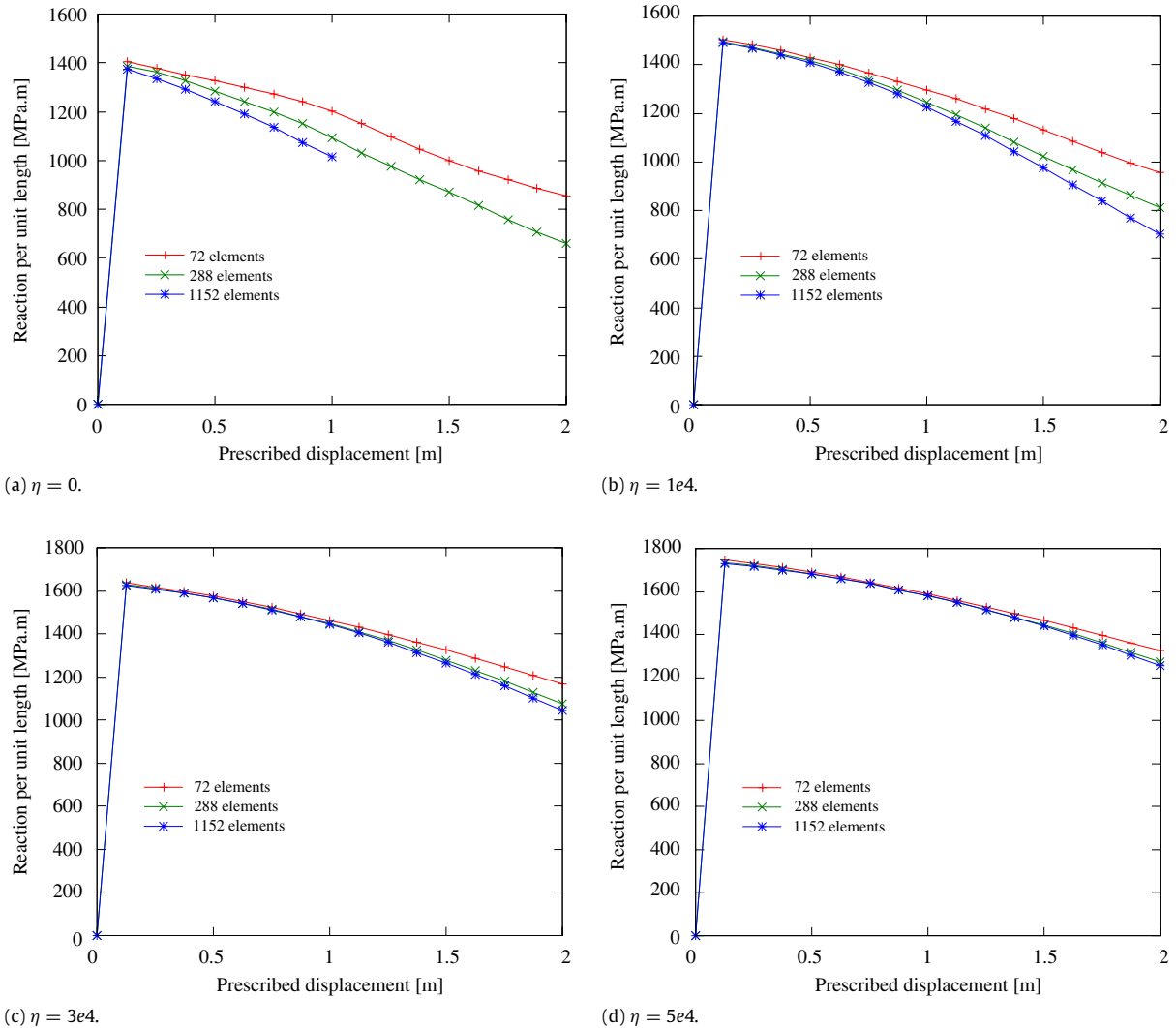


Fig. 6. P vs u graphs for different meshes considered and $\eta = 0, 1e4, 3e4, 5e4$.

most refined mesh has 1152 elements based on two 24×24 elements zones. The material data considered for the mesh sensitivity study is a generalized Perzyna type with $n = \infty$ and $m = 1$. Viscosity parameter values are $\eta = 0, 1e4, 3e4, 5e4$. All the other material data are equal to the case simulated in Section 5.

Fig. 5 shows the deformed configurations for the three different finite element meshes considered, for $\eta = 0$ and an imposed displacement $u = 1$. As can be seen in the pictures a rather marked necking can be observed in the central zone. It is important to present a comparison of the obtained results in terms of the applied force versus displacement graphs. The model response is shown in Fig. 6(a)–(d) for $\eta = 0, 1e4, 3e4, 5e4$ respectively.

Fig. 6(a) displays the response for the inviscid solution $\eta = 0$. As can be easily seen the decreasing part of the curves are significantly distinct for the three considered meshes. The coarsest mesh behaves in a much stiffer way than the more refined ones as expected. The most refined mesh failed to converge after an imposed displacement approximately equal to $u = 1$ m due to severe element distortions close to the central hole.

Results for $\eta = 1e4$ are presented in Fig. 6(b). In this case all results agree fairly better than in the inviscid case. Still in this case the 72 element mesh behaves in a stiffer way and its post peak curve drifts away from the two other curves from $u = 0.5$ m approximately. On the other hand the two most refined meshes show a very reasonable agreement till an imposed displacement of $u = 1$ m. For the larger values of viscosity considered $\eta = 3e4, 5e4$, the obtained results become more and more mesh independent, as can be seen in Fig. 6(c) and (d). The postpeak curves drift away for larger values of u and the computed final loads are quite similar for these two cases.

It is important to point out that the chosen values for viscosity parameter η are small enough in order to reproduce a global softening response for all the studies conducted. From a practical point of view we can say that the added viscosity has a regularizing effect on the model behavior. So, even for viscosity values that are quite limited, and thus far from delivering

a result close to the elastic solution (see Figs. 2 and 3(a)), one can see that the proposed methodology delivers a solution that becomes mesh-independent for a reasonable discretization.

Thus the viscoplastic model, even for low viscosity values, presents rather insensitive results in terms of the chosen finite element mesh. Moreover from a numerical point of view, the hardening modulus h is replaced by a fictitious hardening coefficient $h^* = h + \frac{\eta}{\Delta t}$. In this case even for a $h < 0$, which correspond to material softening, the material can be stabilized adding a proper viscosity value. In summary from the studies conducted we can conclude that results are quite insensitive to the finite element mesh chosen for the viscoplastic response. However, in the case of a rate independent material, results become sensitive again. Possibly the behavior of rate independent models can be explained in terms of elastic perfect plastic model ($h = 0$) tested in this case. In previous works, hardening materials ($h > 0$) simulations performed did not present sensitivity of the computed results in terms of finite element mesh changes [17].

7. Conclusions

Theoretical formulation and numerical implementation of a large strain viscoplastic model have been presented. The structure of the elasto-viscoplastic model is based on hyperelasticity while internal variables theory is maintained. The viscoplastic problem is easily taken into account due to the uncoupled structure of the free energy function.

Consequently the structure of the numerical scheme previously developed for elastoplastic problems is preserved. The elastic predictor problem remains with no changes and the viscoplastic corrector step encompasses the structure of plastic corrector when the stress update algorithm is recast in terms of kinematics variables. In this way the numerical format of the problem naturally includes viscoplasticity.

The stress update procedure is easily solved using a local non linear iterative procedure at the integration point level for the general case. Various closed form expressions can be derived for different particular cases. The discussed procedure recovers the results of the classical radial return algorithm for the inviscid case. Consequently all the advantages that can be obtained from the radial return method like simplicity, robustness and computational efficiency including the consistent tangent operator are maintained.

The numerical example presented has been discussed in the literature, for the small strain regime in most of the cases. In order to verify the behavior of the proposed model several cases with different values of the viscosity parameter η and the rate sensitivity parameter m were simulated in the presence of large strains. From the results obtained, the influence of both parameter was distinguished concluding that m just magnifies the η effect. The limiting elastoplastic case (for $\eta = 0$) and elastic one (for $\eta \rightarrow \infty$) are verified as well.

A mesh sensitivity study has been conducted. From the obtained results we can conclude that results are quite insensitive to the finite element mesh chosen for the viscoplastic response. However, in the case of a rate independent material, results become sensitive again, possibly due to the elastic perfectly plastic material that was tested i.e. exhibiting no hardening ($h = 0$).

References

- [1] C. García Garino, J. Oliver, Un modelo constitutivo para el análisis de sólidos sometidos a grandes deformaciones, parte i formulación teórica y aplicación a metales, *Rev. Internac. Métod. Numér. Cál. Diseñ. Ingr.* 11 (1995) 105–122.
- [2] C. García Garino, J. Oliver, Un modelo constitutivo para el análisis de sólidos sometidos a grandes deformaciones, parte ii implementación numérica y aplicaciones, *Rev. Internac. Métod. Numér. Cál. Diseñ. Ingr.* 12 (1996) 147–169.
- [3] J. Simo, M. Ortiz, A unified approach to finite deformation elastoplastic analysis based on the use hiperelastic constitutive equation, *Comput. Methods. Appl. Mech. Engrg.* 49 (1985) 221–245.
- [4] J. Simo, A framework for finite strain elastoplasticity based on maximum plastic dissipation and the multiplicative decomposition: part i, continuum formulation, *Comput. Methods. Appl. Mech. Engrg.* 66 (1988) 199–219.
- [5] J. Simo, A framework for finite strain elastoplasticity based on maximum plastic dissipation and the multiplicative decomposition, part ii: computational aspects, *Comput. Methods. Appl. Mech. Engrg.* 68 (1988) 1–31.
- [6] J.-P. Ponthot, Unified stress update algorithm for the numerical simulation of large deformation elasto-plastic and elasto-viscoplastic processes, *Int. J. Plast.* 18 (2002) 91–126.
- [7] P. Perzyna, Fundamental problems visco-plasticity, in: G. Kuerti (Ed.), *Advances in Applied Mechanics*, Vol. 9, Academic Press, 1966, pp. 243–377.
- [8] J. Lubliner, *Plasticity Theory*, Macmillan, New York, USA, 1990.
- [9] N. Ottosen, M. Ristinmaa, *The Mechanics of Constitutive Modelling*, Elsevier, 2005.
- [10] J. Simo, T. Hughes, *Computational Inelasticity*, Springer Verlag, 1998.
- [11] A. Carosio, K. Willam, G. Etse, On the consistency of viscoplastic formulations, *Int. J. Solids Struct.* 37 (2000) 7349–7369.
- [12] G. Alfano, F. De Angelis, L. Rosati, General solution procedures in elasto-viscoplasticity, *Comput. Methods. Appl. Mech. Engrg.* 190 (2001) 5123–5147.
- [13] W.M. Wang, L.J. Sluys, Formulation of an implicit algorithm for finite deformation viscoplasticity, *Int. J. Solids Struct.* 37 (2000) 7329–7348.
- [14] E. Lee, Elastic-plastic deformation at finite strains, *ASME J. Appl. Mech.* 36 (1969) 1–6.
- [15] J. Nagtegaal, On the implementation of inelastic constitutive equations with special reference to large deformation problems, *Comput. Methods. Appl. Mech. Engrg.* 33 (1982) 469–484.
- [16] E. Marsden, T. Hughes, *Mathematical Foundations of Elasticity*, Prentice-Hall, 1983.
- [17] C. García Garino, F. Gabaldón, J. Goicolea, Finite element simulation of simple tension test, *Finite Elem. Anal. Des.* 42 (2006) 1187–1197.